4 Electrochemical Sensor Applications to the Study of Molecular Physiology and Analyte Flux in Plants

MARK A. MESSERLI,[1] KENNETH R. ROBINSON,[2] PETER J.S. SMITH[1]

4.1 Introduction

Electrophysiological studies on plants have always been challenging. Cell walls and turgor pressure have made it difficult to apply many standard approaches used on animal cells. For these reasons, plant physiologists have long sought and developed novel methods for examining cellular physiology via non-invasive approaches. This review covers one such example, an electrochemical method that evolved out of a series of capacitively coupled techniques using a modulation approach. The first, for biological applications, was published by Blüh and Scott (1950) using an aerial probe. Although sparse on results, the authors claim preliminary data mapping surface potentials from various plant materials. Further development was reported in a series of papers by Grahm (1964) and Grahm and Hertz (1962, 1964) with data on the geoelectric and auxin-induced effects from coleoptiles using parallel plate capacitors. More recently, a more refined device, termed the bioKelvin probe, measured light-induced field changes originating from subsurface currents of a single corn coleoptile (Baikie et al. 1999). This device incorporated positional feedback and improved spatial resolution. Sanger et al. (1990) published a preliminary report using a similar approach.

The biggest breakthrough in the design of an instrument for monitoring external voltage fields, as related to the transmembrane passage of ions, came with the full development of the vibrating voltage probe by Jaffe and Nuccitelli (1974). Davies (1966) briefly described a similar device applied to muscle fibers. While subsequent studies by Jaffe, colleagues, and others are too numerous to mention, the vibrating probe was put to good use by plant physiologists as a method for monitoring ion transport (reviewed by Nuccitelli 1991).

Although a powerful tool, used to great effect on studies involving patterning and tip growth, the voltage probe has the limitation of not being chemically selective. An approach was needed where identification of the transported ion(s) that generated the current could be achieved. The first example was published by Gow et al. (1984), measuring H^+ gradients over the

[1] BioCurrents Research Center, Program in Molecular Physiology, Marine Biological Laboratory, 7 MBL Street, Woods Hole, MA 02543, USA

[2] Department of Biological Sciences, Purdue University, West Lafayette, IN 47907, USA

Plant Electrophysiology - Theory & Methods (ed. by Volkov)

surface of growing hyphae, with the landmark paper by Jaffe and Levy (1987) automating the process for Ca^{2+} measurement. The full description was published by Kühtreiber and Jaffe (1990), with diversification to K^+, H^+, and Ca^{2+} fluxes in maize roots and maize suspension cells by Kochian et al. (1992). Around the same time, further plant applications were being explored by Newman and colleagues (Arif and Newman 1993). The use of ion-selective electrodes (ISEs) in this configuration is termed self-referencing by the authors (Smith et al. 1999). Over the approximately 20 years since its development there have been numerous successful applications and diversification to include other liquid membrane sensors, Cd^{2+} for example (Pineros et al. 1998) and Cl^- (Shabala and Newman 1998; Shabala et al. 2000). Cl^- detection is of particular interest to this review, and will be considered below as detection with the available Cl^--selective solvents is problematic, as recognized by Doughty and Langton (2001), Messerli et al. (2004), and Garber et al. (2005). The use of these sensors highlights the problems and pitfalls that can befall the unwary investigator in applying any electrochemical sensor.

Following the potentiometric ISEs came the self-referencing amperometric design, first applied to oxygen detection (Land et al. 1999; Mancuso et al. 2000). These solid-state redox-based sensors have so far seen a broader application in the animal sciences, but the potential to measure nitric oxide flux (Kumar et al. 2001; Porterfield et al. 2001) or H_2O_2 efflux (Twig et al. 2001, 2005) offers a clear application in plants. Modification through enzyme incorporation has also been demonstrated (Jung et al. 2001).

Electrochemical sensors, when used correctly on biological systems, offer a huge experimental return, particularly in the plant sciences where more conventional electrophysiological approaches are difficult. The self-referencing approach enhances this return by providing flux data and powerful signal analysis, refining sensitivity and selectivity. This review aims to introduce the reader to both the strengths and the weaknesses of this technique, which, although now 2 decades old, may still be unfamiliar to many.

4.2 Electrochemical detection with microelectrodes

4.2.1 Properties of electrochemical sensors

Self-referencing with electrochemical sensors is a modulation technique where a single sensor is used to measure the activity/ concentration of an analyte at different points in space and time. As micron-sized electrochemical sensors are the basis for self-referencing, we will discuss some physical properties of these sensors before discussing their use in a self-referencing mode.

The two fundamental types of micro-electrochemical sensors used with self-referencing to date are the potentiometric, ion-selective electrodes (ISEs), and the amperometric microelectrodes. The ISEs are based on an ion-selective

solvent or liquid membrane, immobilized in the tip of a micropipette with tip diameters of 1–4 μm. For an ideal electrode the measured voltage is related to the activity of the ion by the Nernst equation

$$E = E_0 + S \log a_i \quad (1)$$

where 'E_0' is the offset (reference) potential, 'S' is the Nernstian slope$=\frac{2.3RT}{z_i F}$ and 'a_i' is the activity of the primary ion. The offset potential is comprised of the many boundary potential and liquid junction potential differences that exist across the circuit comprising the reference and measuring electrodes. Through calibration of each ISE we perform an empirical determination of the slope of the line describing the voltage output for the change in ionic activity. Since ionic activity is directly proportional to ion concentration, via the activity coefficient, and the changes that occur to the activity coefficient due to changes in ionic strength are usually negligible during self-referencing, we will use concentration in place of activity for ISEs.

The amperometric sensors are solid-state sensors with usually a metal, platinum or gold, or carbon as the electrolytic surface. The amperometric sensors used in combination with self-referencing, have only been used in constant-potential mode, where the sensors are voltage-clamped to a known potential, relative to the bath potential, that is sufficient to electrolyze the analyte. It is one of the amperometric methods that provides sub-second temporal resolution, but by itself cannot identify the electroactive analyte (Phillips and Wightman 2003). The electrodes are built in a manner that diffusion of the analyte to the electrolytic surface is rate limiting, creating a current that is dependent on the concentration of the analyte

$$I = I_0 + S \cdot C \quad (2)$$

'I_0' is a current offset, 'S' is the slope of the calibration curve with units of Ampere/ Molar, and 'C' is the concentration of the analyte. In special cases of enzyme-based sensors, an electroactive product of the enzyme is measured. The concentration of that product is proportional to the concentration of the non-electroactive substrate of the enzyme (Jung et al. 2001) and thus the concentration of that substrate can be determined.

4.2.2 Response time

General properties of micron-sized sensors (<10 μm) are that they reach equilibrium relatively quickly, have greater spatial resolution, and are much less disturbing to the local chemical environment compared to macroelectrodes. The response times of ion-selective microelectrodes can be so fast that the electronics of the system slow the measured response (Ammann 1986). For example, the response time of potentiometric electrodes will depend on their ability to supply enough charge to the voltage-sensing node in order for

it to reach its steady state value. Low input impedance of the amplifier and stray capacitances in the circuit will draw more charge than an ideal system therefore slowing the response time of the system. Micron-sized, ion-selective sensors have been characterized with high resistances, 1–20 GΩ (Ammann 1986). Amplifier input impedances of 10^5–10^6 GΩ are typically used to minimize current and allow sampling of the ion concentration without dramatically changing it. With an ideal amplifier, why are the electrodes so fast? Diffusion through the stagnant aqueous layer at the surface of the electrode defines the response time of the sensors when the ion-selective membrane is equilibrated with the salt of an ion to which the electrode responds (Bakker et al. 1997). A brief theoretical analysis will put this in perspective. In a diffusion-limited system, how quickly will an analyte diffuse from the edge to the center of the microelectrode? For a 4 μm diameter sensor, K^+, for example, would require only 0.3 ms ($t=L^2/6D$ for diffusion in 3 dimensions, $D_{K+}= 2.0\times10^{-5}$ cm/s). For comparison, it would take 21 s to diffuse from the edge to the center of a 1 mm diameter sensor. Most analytes that have been measured with self-referencing systems have diffusion coefficients in the range of 10^{-4}–10^{-6} cm^2/s indicating that the electronics will be the primary factor limiting the response time of the measurement under relatively ideal conditions.

The response time of ISEs is governed by the ability to provide charge to the sensing node. This involves the availability of charge carriers at the surface of the electrode tip. Therefore, surface area of the ion-selective solvent, proportional to the square of the tip diameter, will affect response time. The presence of interferents will also slow response times. We have characterized the response times of micro electrochemical sensors with our system with different tip diameters, column lengths, and in the presence of an interferent. Figure 4.1A shows an example of the response times for a K^+-selective electrode in a simple solution (100 mM HEPES pH 7 with 0.1, 1 and 10 mM KCl). Figure 4.1B shows an enlargement of the response time from 1 to 0.1 mM K^+, indicated in Fig. 4.1A, and an overlay under the same conditions with the addition of Na^+, a known, albeit poor interferent. These 2–3 μm K^+-selective electrodes respond to 95% of their new steady state value ($t_{95\%}$) in 41–77 ms, depending on the change in concentration (line 3, Table 4.1). The electrode possesses $10^{3.9}$ selectivity for K^+ over Na^+, indicating that a lot of Na^+ must be present to interfere with K^+ detection. In the presence of 450 mM Na^+ (seawater levels) not only does the response time increase nearly 3-fold but the Nernstian response also decreases by 8% (Fig. 4.1B). Both of these features are classic indications of an interferent (Fleet et al. 1974; Bakker et al. 1997). In Table 4.1 we give a listing of the response times of three of the potentiometric sensors and one of the amperometric sensors in defined media. Simple solutions were used in media 1 and 3 to show the effects on response time with changes in tip size and column length. The sensors remained stationary during the experiment, while two to three adjacent streams of media (1 ml/min) were rapidly positioned in front of the measuring electrode. The rapid exchange system was able to exchange streams in front of the measuring electrodes in less than 8 ms ($t_{95\%}$). These measurements describe the response time of the entire measuring system

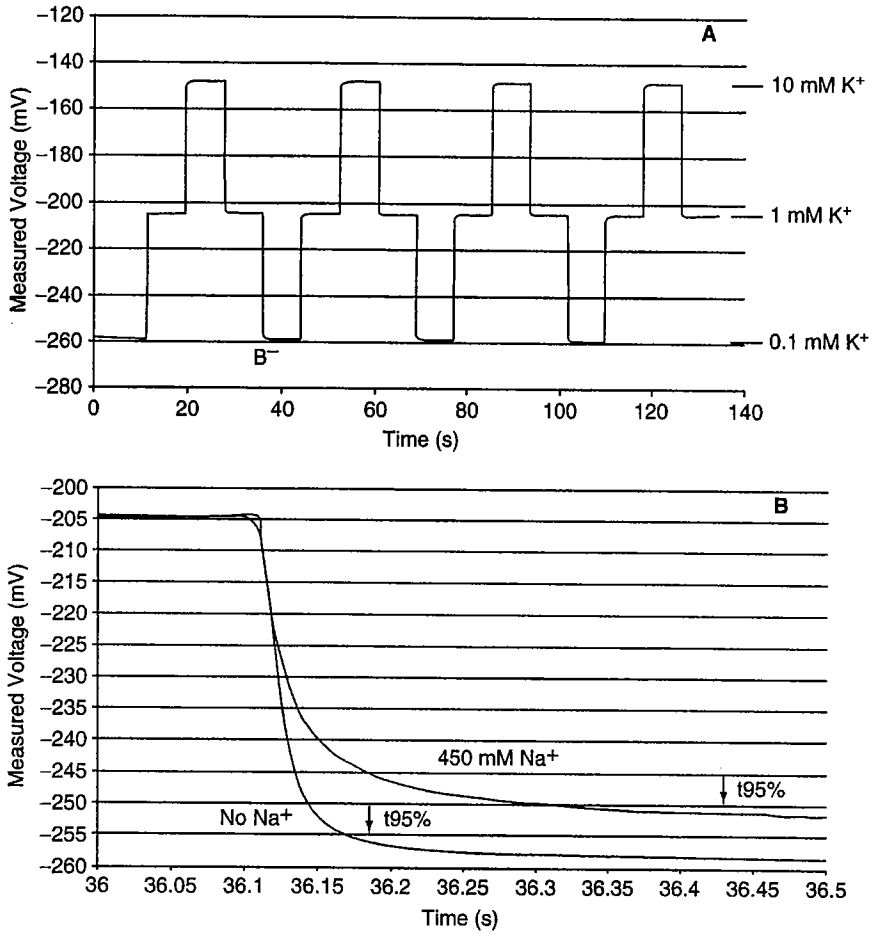

Fig. 4.1. Voltage response of a K^+-selective electrode to step changes in K^+ concentration. A The voltage response recorded by a K^+-selective electrode as a simple medium containing 100 mM HEPES (pH 7.0) with 0.1, 1 or 10 mM KCl was passed over the tip with a rapid exchange flow system. B An overlay of the magnified voltage response from 1 to 0.1 mM KCl, marked in A with a response under similar conditions in the presence of 450 mM NaCl. Na^+ is a characterized interferent of the K^+-selective electrode used here. In the presence of Na^+, the response time is nearly 3 times longer and causes the electrode to respond to this change in K^+ concentration 8% lower than optimal

from the sensor through the electronics for four electrodes of each type. The response times are generally faster than 200 ms for electrodes with tips greater than 1 µm. A few trends can be distinguished:

1) Longer column lengths give rise to longer response times;
2) 2–3 µm diameter pipette tips are faster than 1 °µm diameter tips;
3) Longer response times occur when measuring in lower concentrations of the primary ion.

Table 4.1. Response times determined for a variety of electrochemical microsensors under different conditions.

Electrode	Column length	Tip size	Medium	Response times ($t_{95\%}$ ms) for concentration ranges			
K^+<?3>	100 µm	~1 µm	1	10–1 mM	1–0.1 mM	0.1–1 mM	1–10 mM
				195 ± 59	376 ± 86	165 ± 41	114 ± 26
	1000 µm	~1 µm	1	369 ± 91	516 ± 86	247 ± 54	191 ± 46
	100 µm	2–3 µm	1	41 ± 3	77 ± 4	53 ± 4	44 ± 3
w/ 450 mM Na+	100 µm	2–3 µm	2	64 ± 9	225 ± 6	91 ± 8	69 ± 15
H^+<?3>	30 µm	~1 µm	3	pH 6–7	pH 7–8	pH 8–7	pH 7–6
				209 ± 12	220 ± 15	214 ± 27	202 ± 13
	300 µm	~1 µm	3	251 ± 21	269 ± 14	245 ± 11	244 ± 17
	30 µm	2–3 µm	3	135 ± 23	130 ± 32	126 ± 30	124 ± 35
Ca^{2+}<?1>	30 µm		4	10–1 mM	1–0.1 mM	0.1–1 mM	1–10 mM
				58 ± 9	81 ± 10	48 ± 7	53 ± 10
O_2<?1>	n.a.	2–3 µm	4	Air – N_2 saturated		N_2 – Air saturated	
				21.8 ± 2.8		24.3 ± 2.6	
H^+ Messerli et al. (1999)<?1>	30 µm	1–2 µm	5	pH 5.5–6.0 223 ± 37	pH 6.0–6.5 252 ± 22	pH 6.5–6.0 214 ± 23	pH 6.0–5.5 223 ± 22
H^+ Feijó et al. (1999)	10–15 µm	1–2 µm	6	727 ± 59	664 ± 69	572 ± 27	738 ± 71

Medium 1. 100 mM HEPES (pH 7.0) with 0.1, 1.0 or 10 mM KCl
Medium 2. Medium 1 with 450 mM NaCl
Medium 3. 100 mM MES (pH 6), 100 mM HEPES (pH 7.8) set with KOH
Medium 4. in mM, 120 NaCl, 5 KCl, 2 $CaCl_2$, 2 $MgCl_2$ 10 HEPES (pH 7.4)
Medium 5. in mM, 0.16 H_3BO_3, 0.127 $Ca(NO_3)_2$, 1.0 KNO_3, 5.0 MES, 292 sucrose, pH 5.5 with KOH (Messerli et al. 1999)
Medium 6. in mM 1.6 H_3BO_3, 0.05 $CaCl_2$, 1.0 KCl, 0.05 MES, 146 sucrose (Feijó et al. 1999)

The response times of the H^+ electrodes do not vary as much as the K^+ or Ca^{2+} electrodes and are not as dependent on column length as the K^+. This may be a result of the H^+ buffer present in solution. The response time of the O_2 electrode is very fast as predicted by Schneiderman and Goldstick (1976).

4.2.3 Spatial resolution

The other useful feature of micron-sized sensors is their spatial resolution. The spatial resolution of potentiometric electrodes is defined by the surface area of the ion-selective solvent. As long as bulk movement of analyte does

not occur, the depth of sensing from the surface of a potentiometric electrode is considered negligible compared to the diameter of the ion-selective solvent itself, usually 1–4 μm. For example, if an electrode was being used to measure ionic concentration at a point near the surface of the cell, a 1–4 μm diameter electrode placed with the surface of the tip orthogonal to the cell surface will report the average concentration over the 1–4 μm tip diameter. Amperometric sensors used in constant potential mode, on the other hand, possess a sensing field that extends out into the medium away from the electrolytic surface. Take for example the O_2-sensing electrode. The electrode generates current by reducing O_2 at its sensing surface. Reduction of O_2 consumes O_2 in the region immediately in front of the tip creating an O_2 depleted zone. These O_2 depleted fields have been modeled for both macro and microelectrodes with recessed and/ or coated tips (Schneiderman and Goldstick 1976, 1978). Carefully constructed electrodes with recessed electrolytic surfaces and/ or coatings will limit the extent of this O_2 depleted field keeping the depletion zone restricted close to the tip. A well-constructed electrode can have virtually the entire O_2 depleted zone located within the membrane at its tip. Therefore, the choice of design and construction of amperometric electrodes will have the greatest influence defining the sensing zone.

In summary, electrochemical detection with microelectrodes under relatively ideal conditions can relay a concentration measurement quickly from a spatially restricted domain.

4.2.4 Electrode types

4.2.4.1 Potentiometric: construction

The manufacturing of micron-sized ISEs used in biological systems has changed little in 2 decades. Briefly, our method involves pulling borosilicate glass capillaries to the appropriate taper and tip size, 1–4 μm, drying the glass at >200 °C, making the glass hydrophobic by exposing it to the vapor of N,N-dimethyltrimethylsilylamine, backfilling with an appropriate electrolyte (some are listed in Table 4.1) and then tip filling with a hydrophobic, ion-selective cocktail to the appropriate length, listed in Table 4.1 for the examples given (for more details, see Smith et al. 1999). The column length was chosen empirically, primarily for stability of the ion-selective solvent in the pipette tip and the response time of the electrode. For the examples given in Table 4.1, the H^+ and Ca^{2+} electrodes are made with a 30 μm column of ion-selective solvent, while the K^+ electrode is made with a 100–150 μm column length. More stable K^+ electrodes can be made with smaller diameter tips. The reason for these differences in stability is probably dependent on the physical properties of the solvents used in the ion-selective cocktail. The solvent used in the H^+ (Sigma-Aldrich/Fluka cat #95293–1EA) and Ca^{2+} (Sigma-Aldrich /Fluka cat # 21048–1EA) cocktails is o-nitrophenyl-n-octyl ether,

which is 3.9 times more viscous and nearly 3 orders of magnitude less soluble in water than 2,3-dimethyl-nitrobenzene (Ammann 1986) that is used as the solvent in the K^+-selective solvent (Sigma-Aldrich/ Fluka cat # 60398–1EA-F). There is certainly flexibility in the column length of the electrodes. Based on resistance changes that occur with increased column lengths (Kühtreiber and Jaffe 1990), it was thought that significant increases in response times would occur as column length increases. The response times for shorter columns, such as 10–30 μm used for the H^+ and Ca^{2+} electrodes change more linearly with column length while the response times for longer column lengths increase in a logarithmic manner with increasing column length. In practice, a slight deviation from the expected length does not change the response time very much, at least when considering the use of these electrodes in the self-referencing application.

The back filling solution is used to provide electrical contact between the back surface of the ion-selective solvent and the voltage-sensing node, via a Ag/AgCl wire. Usually a 100 mM solution of the ion being measured is used as the backfill in order to ensure that the ionic concentration between the back of the ion-selective solvent and the backfilling solution does not change. If large amounts of the ion being monitored enter the ion-selective solvent and pass through to the backfilling solution, the voltage recorded by the amplifier will be dependent on both changes. The backfilling solution should also be closely matched osmotically to the bath solution. Osmotic gradients across the ion-selective solvent can lead to movement of ion-selective solvent into or out of the electrode tip, either causing the electrode to fail or increase noise.

4.2.4.2 Potentiometric: selectivity

Selectivity of the electrode is the single most critical factor when performing measurements in complex media. How well does a particular electrode sense the primary ion of interest versus all other ions in solution? While the manufacturer lists many interfering ions there are also many other commonly present ions that may cause interference, which have not been tested. Figure 4.2 shows how an interfering ion will reduce the sensitivity of an ISE for its primary ion. Figure 4.2 compares the relationship of voltage to primary ion concentration for a relatively ideal electrode determined with the modified Nernst equation (solid) to the voltage of the primary ion concentration in the presence of different levels of an interfering ion (dashed) determined with the modified Nicolsky–Eisenman equation. The Nicolsky–Eisenman equation in the upper left of Fig. 4.2 has the addition of the concentration of the interfering ion (C_j) and the selectivity factor K_{ij}, compared to the Nernst equation in the lower right. The Nicolsky–Eisenman equation assumes that the response of the electrode is Nernstian for the interfering ion. For this comparison both primary and interfering ions are monovalent and only one interfering ion is present even though the equation can be used to accommodate many

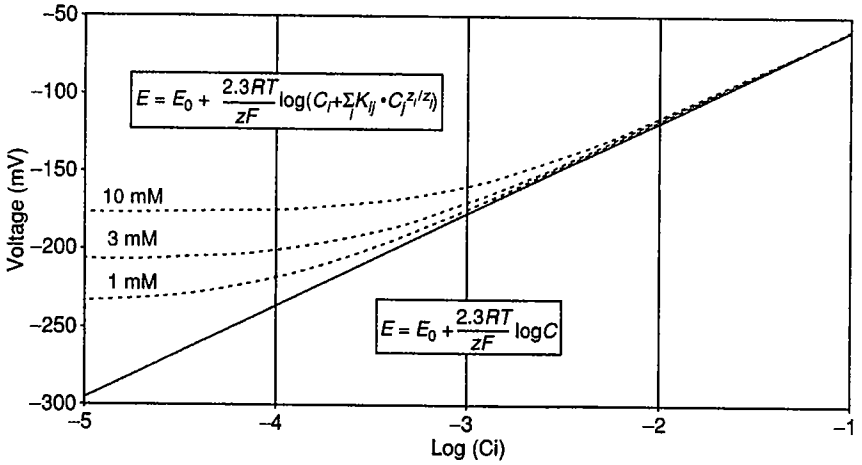

Fig. 4.2. Predicted voltage response for changes in primary ion concentration for a monovalent cation in the absence and presence of different concentrations of a monovalent cation interferent. A modified Nernst equation, listed in the lower right, was used to model the voltage response under ideal conditions for changes in the primary ion concentration (*bold*). A modified Nicolsky–Eisenman equation, listed in the upper left, was used to predict the voltage response for changes in the primary ion concentration in the presence of an interfering ion. The interfering ion concentrations are listed above their respective curves. The selectivity coefficient, K_{ij}, used for this model was 0.1, i.e. the solvent is 10 times more selective for the primary ion than the interfering ion

interfering ions. By comparing the responses of an ideal electrode to one that senses an interfering ion, it can be shown that under circumstances where $K_{ij} \cdot C_j$ is small compared to C_i, the slope approaches the Nernstian value and will remain relatively constant over small differences in primary ion concentration. However, in circumstances where $K_{ij} \cdot C_j$ is large compared to C_i, the slope approaches zero, yielding an electrode that is insensitive to changes in the primary ion concentration. Interfering ions not only reduce the electrode's voltage response to the primary ion but they also slow the response time of the electrode as shown in Fig. 4.1B. This point is particularly important when using the electrodes in self-referencing mode where a temporal component is part of the modulation approach. This will be addressed below.

In biological applications, it is critical for the investigator to empirically test the voltage response and response time of an ISE in the medium in which the experiments are to be performed. Simple solutions of the primary ion are not sufficient. If cellular poisons are to be added, then the electrode must be tested in the presence of those poisons as well. Considering the application of Cl^- sensors provides an example of some problems encountered for one of the ion-selective solvents with poor selectivity. Recently, Zonia et al. (2002) made the rather startling discovery that large Cl^- fluxes were an integral component of pollen tube extension (see "Self-referencing as applied to plants"

below). They used a commercially available Cl^--selective exchanger (Sigma-Aldrich/Fluka cat. #24899). Measurements were performed in the presence of two interferents that were not identified. Sulfonates are listed as interferents for this Cl^--selective cocktail which has less than 1 order of magnitude selectivity for Cl^- over methylsulfonate (Fluka Chemical Corp. 1996; Messerli et al. 2004). However, it may not be so apparent that most of the Good Buffers, specifically 2-(N-Morpholino)ethanesulfonic acid (MES), contain sulfonates and that the Cl^- channel blocker, 4,4′-diisothiocyanatostilbene-2,2′disulfonic acid disodium (DIDS) contains sulfonates. Both compounds were used in the Zonia et al. (2002) studies. It was later determined that the Cl^- electrode had only 2.4-fold selectivity for Cl^- over the anionic form of MES, indicating that the Cl^- electrode can indirectly monitor pH gradients (Messerli et al. 2004). Another Cl^--selective cocktail (Sigma-Aldrich/Fluka cat. 24902) is directly sensitive to pH at low Cl^- (Garber et al. 2005). Consideration of the previously characterized H^+ fluxes in lily pollen grains and tubes (Feijó et al. 1999; Messerli et al. 1999) as well as the poor anion selectivity of the Cl^- electrode, indicates that the putative Cl^- fluxes are in fact changes in the anionic concentration of the buffer due to H^+ gradients and not changes in Cl^- concentration (Messerli et al. 2004). It was also found that in the presence of 100 μM DIDS the electrodes responses to Cl^- drop by 63% on average between 0.1 and 1 mM Cl^- (Messerli et al. 2004). Zonia et al. (2002) measured an 80% drop in Cl^- efflux from a tobacco pollen tube in the presence of 80 μM DIDS and a background Cl^- concentration of 0.4 mM. The decrease in the Cl^- flux measurement can be accounted for by the decreased sensitivity of the electrode with the added interferent.

It should be clear from the examples discussed above that careful testing must be performed in order to determine how an ISE will perform in complex media and in the presence of reagents used to modify cellular activity.

4.2.4.3 Potentiometric: positional artifacts

The positioning of ISEs near surfaces can generate artifacts. Of particular relevance is the current driven and zero-current ion flux emanating from the tip of the sensor. Although our tip sizes are small and the static boundary layer limited in size, ions escaping to the bulk could accumulate between the probe tip and the target cell or tissue. Abnormal, apparent, biological fluxes have been seen for Ca^{2+} when Ca^{2+}-selective electrodes are brought within 1–2 μm of a membrane or an insulating surface when the background Ca^{2+} concentration is <1 mM. The source of this artifact is a combination of current leakage from the electronics supplying charge to the ion-selective solvent and zero-current (electroneutral) ion exchange of the primary ion for an interfering ion. This phenomenon has been shown for K^+ and Ca^{2+}-selective solvents (Mathison and Bakker 1998; Lindner et al. 1999). The artifacts are most apparent in solutions of low background primary ion. Reducing the concentration

of the primary ion in the backfilling solution has been one method of reducing the ion leak (Mathison and Bakker 1998). Additionally, an applied current can control the flux across the membrane counteracting the spontaneous zero-current ion flux (Lindner et al. 1999). Pergel et al. (2001) used a current to compensate for the zero current phenomenon discussed with Pb^{2+} detection. By reducing if not eliminating the leakage of Pb^{2+} out of the electrode tip, the authors were able to maintain a Nernstian response down to 3 pM.

4.2.4.4 Amperometric: construction

A number of solid-state amperometric microelectrodes have been used in the self-referencing mode. Two different metal electrode configurations have been used. These include gold-plated Woods metal (Diamond General Co., Ann Arbor, Mich., USA) for the detection of O_2, and a platinum disk microelectrode for the measurement of O_2 (Jung et al. 2000a,b) and H_2O_2 (Twig et al. 2001, 2005). Carbon fiber-based microelectrodes have been used for the detection of nitric oxide (NO) (Kumar et al. 2001; Porterfield et al. 2001) and ascorbic acid (Pepperell et al. 2003). More complex enzyme-based microelectrodes have been fashioned to measure gradients of glucose (Jung et al. 2001) and glutamate (Bogorff et al. 2003). We will briefly discuss the fabrication of the first three types of electrodes.

The gold-plated Woods metal microelectrode dates back to the early days of O_2 microelectrodes (Whalen et al. 1967). The low melting temperature Woods metal is heated above melting, forced to the tip of the pulled micropipette by back pressure, etched back into the glass pipette and then electroplated with gold or gold and then platinum to build a recessed electrolytic surface for the reduction of O_2. The recessed tip creates an O_2 diffusion-limited sensor and prevents the O_2 depleted field from extending away from the sensor tip out into the bulk medium (Schniederman and Goldstick 1976, 1978). When the electrode is built such that the O_2-depleted field remains close to the electrode tip, the response time of the electrode can be tens of milliseconds (Schneiderman and Goldstick 1976), which we have achieved with the platinum-based O_2 sensors shown at the bottom of Table 4.1.

The platinum-based sensors are made by etching 25 μm diameter, platinum wire to a tip of about 1–3 μm diameter, inserting the etched wire into a micropipette similar to those used with the ISEs, immobilizing the platinum wire in the micropipette with a UV or heat curing epoxy, and then etching a second time to recess the electrolytic platinum surface (Jung et al. 2000a,b). Coated tips can help reduce the external O_2 depleted field and provide some added selectivity. Buerk (2004) provides an excellent overview of oxygen microelectrodes, their design and function.

Carbon fiber microelectrodes are made in a similar manner as the platinum wire electrodes. A fine carbon fiber 5–8 μm diameter is positioned near the tip of a finely pulled pipette tip and cemented into place with a UV or heat

curing epoxy. The carbon fiber electrode is then beveled to expose a cross-sectional surface of the fiber. Coatings are used to help impart selectivity (Friedemann et al. 1996).

4.2.4.5 Amperometric: selectivity

A constant polarization potential is applied to amperometric sensors to oxidize or reduce the analyte. The current generated is proportional to the concentration of the analyte. However the potential can oxidize or reduce other compounds in solution that are electrolyzed at or below the electrode holding potential. For example, nitric oxide (NO) oxidation at a carbon fiber begins to plateau between +0.8 to +0.9 V (Zhang et al. 2002). Neurotransmitters, ascorbic acid, nitrite and H_2O_2 can also be oxidized at this high voltage. A charged coating on the carbon fiber surface can eliminate passage of charged compounds (Friedemann et al. 1996; Zhang et al. 2002). However, H_2O_2, an uncharged molecule, will be oxidized as it can pass through the coatings. Addition of a layer of catalase to the charged coating layers, similar to the enzyme layers used by Csöregi et al. (1994), can eliminate H_2O_2 before it has chance to reach the electrolytic surface. Multiple coatings on a microelectrode will decrease sensitivity by reducing electrolytic surface area and slow response time by impeding diffusion of the analyte.

Another common problem with amperometric sensors is that they are strongly dependent on pH. One only has to look at a standard reduction potential table to see that H^+ consumption is involved with most every reaction. Take, for instance, O_2 reduction: $2O_2+4H^++4e\text{-}2H_2O$. The rate of this reaction at a bare micro Pt disk electrode will be dependent on the limiting factor which should be diffusion of O_2 to the electrolytic surface. In practice this is not the case and the O_2 sensor can very quickly become a good H^+ sensor. Certainly the recessed tip, coated, Wood's metal electrodes purchased from Diamond General Co. can sense pH gradients (Messerli and Robinson, unpublished observations).

4.2.4.6 Amperometric: positional artifacts

In amperometric applications, the analyte is actually being consumed on the electrode surface. Therefore, an analyte depletion zone can form. An ideal electrode is built such that the analyte-depleted region is located primarily within the electrode itself. However, it can quickly be envisioned that even a small depletion of the analyte in the bulk can give rise to a measurement artifact. In the extreme case, placing the electrode up against an insulator will prevent any analyte from reaching the surface of the electrode resulting in no change in current for a change in analyte. Backing the electrode away from the insulator such that analyte can now diffuse, albeit in a restricted manner, will still give rise to a value below the real level. Moving back further, such

that diffusion of analyte is not impeded, will result in maximal current for a change in analyte concentration.

A second possible source of artifact is that reaction products can accumulate at the electrode surface when diffusion is restricted by the target. A good example of this comes from the study of Jung et al. (2001) during the development of the self-referencing glucose probe. This design incorporates glucose oxidase and measures glucose concentration indirectly though the production of H_2O_2. As long as glucose is present the glucose oxidase at the tip of the electrode will produce H_2O_2. The H_2O_2 that diffuses toward the electrolytic surface will be measured but the H_2O_2 that diffuses out into the bulk medium will be lost. However, in this case when the electrode came into close proximity to a HIT cell cluster (hamster insulinoma tumor) it appeared as if the cell was releasing glucose. Although this would have been an exciting result, the better hypothesis was the presence of an artifact–, probably the accumulation of the H_2O_2 when the sensor was close to the source. A similar response, glucose production by a solid glass bead, confirmed H_2O_2 accumulation as the source of the artifact. In the biological application, the addition of catalase to remove sensor generated H_2O_2, converted apparent glucose efflux to the expected glucose influx.

Therefore, in practice the investigator is wise to assess the extent of these depletion and restrictive diffusion zones.

4.3 Self-referencing

4.3.1 Introduction

Self-referencing, with electrochemical sensors, is a modulation technique used to measure the concentration of an analyte at two positions within a chemical gradient of the analyte. The term self-referencing refers to the fact that the concentration measurements, collected by the single sensor are compared to each other in order to determine the concentration difference between the two points. Each sensor has its own bath reference electrode. Commonly, the gradients that are measured with this technique exist along a path orthogonal to the cell/ tissue surface so the electrochemical sensor is oscillated repeatedly between two points, one closer to the cell (near pole) and one a set distance away (far pole), usually 10 μm. Figure 4.3 shows a potentiometric, ISE in both the far pole (top) and near pole (bottom) of translation near a growing lily pollen tube tip. Both potentiometric, ISEs and amperometric sensors have been used in this manner. The electrodes are translated between the two poles at a frequency of about 0.3 Hz, collecting an analyte concentration measurement at each pole. The difference in analyte concentration between the two poles can be used to calculate the flux of the analyte. While this sort of measurement could be achieved with two similar, stationary sensors, positioned at

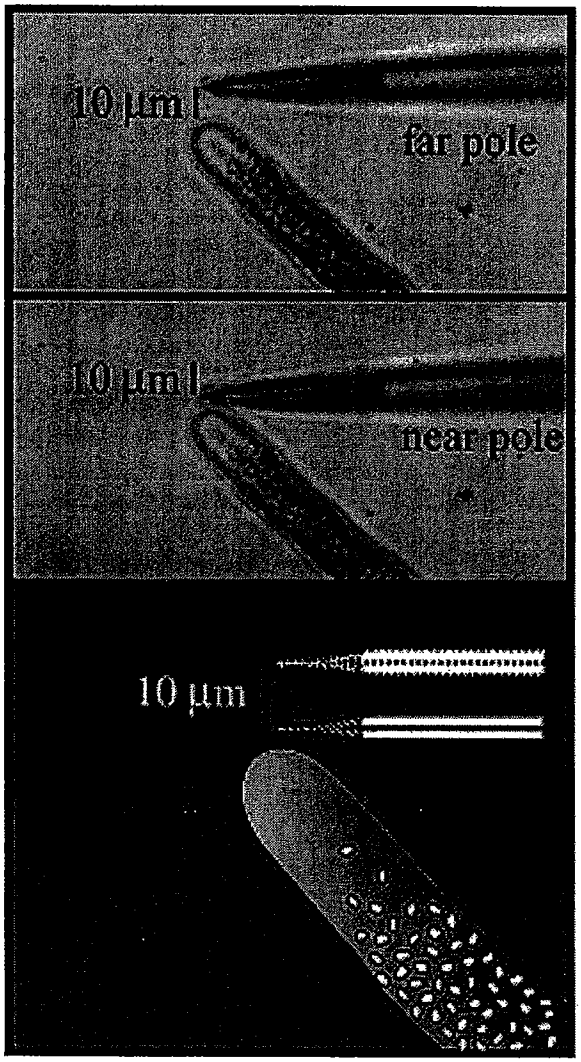

Fig. 4.3. Images of an ion-selective electrode during self-referencing measurements acquired at the tip of a growing pollen tube. The top image was acquired when the electrode was at the far pole of excursion while the middle image was acquired when the electrode moved to the near pole of excursion. The bottom image shows a conceptual representation of the electrode measuring at two points within the concentration gradient of the primary ion

known distances from the source, the system would suffer from the signal drift and noise inherent to two separate measuring systems. In a single electrode system, the effects of drift and noise can be minimized over time by regularly comparing the measurements between the two poles of excursion. Here lies one of the single most powerful reasons for using self-referencing, the

minimization of system drift and noise on analyte detection. We will first address the modulation of potentiometric sensors and then make direct comparison with modulation of amperometric sensors.

4.3.2 Self-referencing of ion-selective electrodes

Minimizing drift and noise for a potentiometric sensor can best be explained by introducing a formulation of the Nernst equation during self-referencing. The voltage difference at the two poles of excursion within the ionic gradient is related to the concentrations at the two poles by the following equation.

$$\begin{aligned} E_1 - E_2 &= (E_0 + S\log C_i)_1 - (E_0 + S\log C_i)_2 \\ \Delta E &= (S\log C_i)_1 - (S\log C_i)_2 \\ \Delta E &= \log C_{i(1)}^{S_1} - \log C_{i(2)}^{S_2} \\ \Delta E &= \log\left(\frac{C_{i(1)}^{S_1}}{C_{i(2)}^{S_2}}\right) \end{aligned} \tag{3}$$

$E_1, C_{i(1)}, S_1$ are the measured voltage, primary ion concentration and slope of the voltage-log(C_i) graph for the near pole of excursion. The subscript 2 has been used to label the same parameters for the far pole of excursion. By calculating the difference in potentials over short periods of time, the slower drifts, due to the constant potential differences throughout the system, are reduced. This places the emphasis of the potential difference measurement on the concentration difference of the ion. An important point should be raised here regarding the sensitivity of detection with regard to the background ion concentration during measurements. $C_{i(1)}$ is the sum of the background ion concentration and the concentration change generated by the source while $C_{i(2)}$, in most cases, is close to the background ion concentration. For a given change in ion concentration due to cellular activity, it is easier to generate a larger ΔE when the background concentration of the measured ion is lower. This has led to the lowering of the background ion concentration in order to generate ΔE with greater signal to noise. Care must be taken to ensure that changing the background concentration does not interfere with normal cellular activity or generate positional artifacts as discussed above.

Equation 3 can be simplified to a general form to determine the relationship between the ionic concentrations at the two points of excursion.

$$C_{i(1)} = C_{i(2)}^{S_2/S_1} \cdot 10^{\Delta E/S_1} \tag{4}$$

We have purposely allowed the slopes at two points of the calibration curve to remain, in order to address measurement of the primary ion under three different circumstances, 1) differential concentration of the primary ion in the absence of an interfering ion 2) differential concentration of the primary ion

in a constant concentration of an interfering ion and 3) differential concentration of a primary ion coexisting with a gradient of an interfering ion.

For an ideal electrode used in the absence of interfering ions, the slope is constant over a wide range of the primary ion concentration, usually described by the manufacturer, and close to the Nernstian slope discussed above in Fig. 4.2, i.e. $S_1=S_2=S$. Therefore, eq. 4 can be simplified to:

$$C_{i\,(1)} = C_{i\,(2)} \cdot 10^{\Delta E/S} \tag{5}$$

Under many circumstances the average concentration of the ion at the far pole, position 2, is not too different from the average concentration of that ion in the bulk solution. Therefore the difference in ion concentration between the two points of excursion can be described as follows.

$$\Delta C = C_{i\,(1)} - C_{i\,(2)} = C_{bath} 10^{\Delta E/S} - C_{bath} \tag{6}$$

A primary assumption here is that the concentration difference measured between the two excursion points is linear. This is only true if the excursion distance is small compared to the extent that the gradient extends out into the bulk solution. For small cells an excursion of 10 µm will most likely sample over a distance in the gradient in which the concentration difference is not linear and therefore will lead the investigator to underestimate the true flux. Incorrect estimation of the true flux could also occur during a two-point measurement in a more intense, extended gradient, where the concentration of the ion in the far pole is substantially different from the background concentration of the ion. In both of these cases, a three-point measurement can be performed in order to 1) more carefully map the concentration gradient with a third point to either ensure a linear relationship or determine a more accurate non-linear relationship and 2) to determine the concentrations in the gradient relative to the background concentration of the ion in the bath. For slow drift conditions the probe can simply be moved from position 3 (outside of the gradient) to position 2 (slightly into the gradient) to position 1 (deeper into the gradient). However, a more precise method is to regularly move between position 3 and positions 2 and 1, so a collection scheme goes from position 3 to 2 to 3 to 1 to 3 and so on.

Measurement of a concentration difference for a primary ion in the presence of a constant concentration of an interfering ion is a more difficult situation. Two variables in eq. 4 need to be determined, specifically the concentration of the ion in the near pole $C_{i(1)}$ and the new slope of the calibration curve in the near pole, S_1. Revisiting Fig. 4.2 gives insight into the problem. With a small $K_{ij} \cdot C_j$ compared to C_i the slope is close to Nernstian and eqs 5 and 6 can be used as discussed above. With a large $K_{ij} \cdot C_j$ compared with C_i the electrode is very insensitive to changes in the primary ion concentration. When the $(K_{ij} \cdot C_j)/C_i$ ratio is 10, the original Nernstian potential is only 10% of its original value and the measurement should probably not be attempted. The use of the electrode under these circumstances will depend on the signal to noise ratio of the system and therefore lies at the discretion of the investigator. For the region in

between these two zones the electrode is responsive to the concentration change in the primary ion concentration but the slope of the line changes with a change in concentration. Therefore, a relationship between the change in voltage and the change in slope needs to be established in order to measure two points in a concentration gradient of a primary ion in the presence of a constant concentration of an interfering ion. In Fig. 4.2 it can be seen that the slope and voltage are closely related in a predictable manner if the selectivity coefficient, K_{ij}, and the background concentration of the interfering ion, C_j, are known, i.e. a single voltage measurement can be used to determine both the slope and the concentration of the primary ion in the near position. We will address the presence of a single interfering ion below. Rearranging the modified Nicolsky–Eisenman equation to get primary ion concentration in terms of voltage and finding $\frac{d}{dE}$ we can determine the relationship of the slope at any point along the curve in terms of voltage.

$$
\begin{aligned}
E &= S_N \cdot \log\left(C_i + K_{ij} \cdot C_j^{z_i/z_j}\right) \\
C_i &= 10^{E/S_N} - K_{ij} \cdot C_j^{z_i/z_j} \\
\log(C_i) &= \log\left(10^{E/S_N} - K_{ij} \cdot C_j^{z_i/z_j}\right) \\
\frac{1}{S} &= \frac{d\log(C_i)}{dE} = \frac{10^{E/S_N}}{S_N\left(10^{E/S_N} - K_{ij} \cdot C_j^{z_i/z_j}\right)}
\end{aligned}
\tag{7}
$$

'S_N' is $\frac{2.3RT}{z_i F}$ and S is the slope along the curve. In order to achieve this sort of measurement we need to know the starting position (voltage point) along the theoretical curve. We can calculate the starting voltage point on the theoretical graph by determining the slope in the bath empirically and solving for E in Eq. 7.

$$
E = S_N \log\left(\frac{S_N \cdot K_{ij} \cdot C_j^{z_i/z_j}}{S_N - S}\right) \tag{8}
$$

From this point on the theoretical curve, a small change in measured voltage, ΔE, either up or down the curve can be used to determine both the new slope at the near pole, eq. 7, and the concentration in the near pole, eq. 4. Equation 6 can now be used to determine the relative concentration difference. If the concentration of the ion in the far position is sufficiently different from the background concentration then a three-point measurement will have to be made, as discussed above. This method of calculation works for the three-point measurement as well.

The final case to consider is measurement of a gradient of a primary ion coexisting with a gradient of an interfering ion. Two variables from eq. 4 need to be determined, specifically the concentration of the primary ion and the

slope of the curve for the primary ion in the near pole. However, now these two variables are not easily predicted as above because the concentration of the interfering ion will influence both variables and the concentration of the interfering ion in the near pole is unknown. Figure 4.2 shows how the concentration of the interfering ion alters the voltage—concentration relationship and changes the slope of the curve. This means that a second ISE for the interfering ion must be used at the same time as the ISE for the primary ion. This will enable measurement of the interfering ion at the near pole and allow prediction of the concentration and slope of the curve for the primary ion in the near pole. If a relatively ideal ISE can be used to measure the interfering ion then the situation discussed above with eq. 7 can be used to solve for the primary ion flux. However, if the ISE used to measure the interfering ion can also sense the primary ion then no simple method to determine the flux of either ion exists.

4.3.3 Self-referencing of amperometric electrodes

Amperometric electrodes have also been used in self-referencing mode incorporating many of the advantages discussed above for the potentiometric electrodes. To date, all of the amperometric sensors have been used in constant potential mode, where the sensor is clamped at a specific holding voltage to oxidize or reduce the analyte. Electrodes are built so that measurement of the analyte is limited by diffusion of the analyte itself, attempting to ensure a current that is dependent on the analyte concentration and not the concentration of a secondary factor or byproduct. The current generated by this redox reaction is therefore proportional to the concentration of the analyte. In the special case of enzyme-based sensors, for instance using glucose oxidase to measure a concentration difference of glucose, a by-product of the enzyme-substrate reaction, H_2O_2, is measured (Jung et al. 2001). Many other forms of amperometric detection exist and are currently under investigation in order to increase the range of analytes than can be measured with self-referencing.

For an ideal electrode under constant holding potential, the measured current is proportional to the concentration of analyte. During self-referencing the differential current can be used to give a measurement of the differential analyte concentration.

$$\begin{aligned} I_1 - I_2 &= \left(I_0 + S \cdot C\right)_1 - \left(I_0 + S \cdot C\right)_2 \\ I_1 - I_2 &= S\left(C_1 - C_2\right) \\ \Delta C &= \frac{\Delta I}{S} \end{aligned} \tag{9}$$

I_1 and C_1 are the current and concentration of the analyte in the near pole of excursion. The subscript 2 has been used to identify the same parameters in the far pole of excursion. S is the slope of the calibration curve. Unlike ISEs, knowing the background concentration of the analyte is not necessary to determine the differential concentration due to the linearity of the current-concentration relationship.

4.3.4 Calculation of flux

To quantify the analyte flux, the differential concentration measurement is converted to flux. This provides a direct means to count the number of molecules passing through a unit area during a unit time. Not only does flux give a value proportional to transport activity but it also can be used to calculate the total amount of analyte uptake or release by integrating the flux over space and time. Flux takes into account the diffusion coefficient of the analyte being measured, the distance over which the differential concentration measurement was acquired, the surface geometry of the source and the distance from the source. For cases where the measuring electrode is relatively close to a large source of the analyte gradient and the differential concentration is measured over a small distance Δx within the gradient, the source can be modeled as a planar source so the flux (J) is

$$J = -D\frac{\Delta C}{\Delta x} \tag{10}$$

where D is the diffusion coefficient of the measured analyte. By this model, the flux measured at some distance from the source is the same as the flux at the surface of the source. What constitutes a planar source? Kochian et al. (1992) found that the planar flux calculation was adequate for H^+ fluxes determine between a 30 μm distance, within 100 μm of a 1 mm diameter root. However, for smaller cells or tissues the geometry of the source must be taken into account (Henriksen et al. 1992; Messerli et al. 1999, 2004). In order to determine flux at the cell surface for known surface geometries it is useful to calculate analyte flow, i.e. the quantity of substance (Q) moving per unit time (Henriksen et al. 1992). Flow is the same for all concentric regions from the source surface. Flux at the source surface is the flow divided by the surface area of the source. Therefore, radially emanating flow from a cylindrical surface is:

$$Flow = \frac{Q}{t} = \frac{2\pi D}{\ln(b/a)}(\Delta C) \tag{11}$$

where D is the diffusion coefficient of the analyte and a and b are the radial distances between the center of the cylinder and the electrode tip at the near and far poles, respectively. These equations have been adapted from Crank (1967). Analyte flux at the surface of the cylinder is then determined by dividing by its surface area $2\pi rl$. A caveat of this approach is the assumption that the flow is equal at all points around the cylinder and along the shaft of the cylinder. An alternative is to calculate flux per unit length by dividing by $2\pi r$ (Henriksen et al. 1992). The flow from a spherical source is

$$Flow = \frac{Q}{t} = 4\pi D\frac{ab}{b-a}(\Delta C) \tag{12}$$

Flux at the cell surface can then be determined by dividing by the sphere surface area $4\pi r^2$. Many researchers have chosen to forgo flux calculations, as they are only interested in changes of the differential concentration measurement for cells and tissues under different conditions. Given that the cells

being used have relatively similar surface geometry and that the electrodes are positioned at a similar position with respect to the cell surface, this simple method is adequate.

4.3.5 Correction for analyte buffering

There are a number of circumstances that cause the calculated flux to be smaller than measured. In the first example discussed here, extracellular buffers can collapse gradients of free analytes. This has been addressed for the collapsing of H^+ gradients by H^+ buffers (Arif et al. 1995; Demarest and Morgan 1995). The analyte can diffuse from the surface of the cell in either its free state or bound to the buffer. ISEs only measure the free concentration of the analyte. The actual H^+ flux from a source is the sum of the measured free H^+ flux and the unmeasured H^+ flux moving as H^+ bound to buffer.

$$J_{Htotal} = J_{Hmeasured} + J_{HB}$$

Knowing the conditions under which the H^+ flux was measured, i.e. $[H^+]$ of medium, Ka of the buffers and concentration of buffers present, a simple relationship can be derived to determine the ratio of H^+ diffusing as bound to buffer compared to the freely diffusing H^+. Arif et al. (1995) and Demarest and Morgan (1995) have derived two separate sets of equations that can be simplified to the same equation given below.

$$x_i = \frac{D_B}{D_{H^+}} \cdot [B] \cdot \frac{Ka}{\left(Ka + [H^+]\right)^2} \tag{13}$$

The correction factor, x_i, is the ratio of the H^+ bound buffer flux to the free H^+ flux. Therefore

$$J_{Htotal} = J_{Hmeasured}\left(1 + x_i + \ldots + x_n\right) \tag{14}$$

where a number of different H^+ buffers ($x_i + \ldots + x_n$) could be carrying H^+ away from the source. The correction factor is based on 3 criteria, the ratio of the diffusion coefficients of the protonated buffer to the proton, the buffer concentration and the Ka of the buffer compared to the $[H^+]$ of the medium. Under most conditions the first term will be relatively constant because buffer sizes and diffusion coefficients do not differ very much. The smaller bicarbonate ion, for example, (M_r 61 $D=1.2\times10^{-5}$ cm/s) will only produce a first term of 0.13. while PIPES (M_r 302 $D=0.52–10^{-5}$ cm/s) one of the largest Good buffers, will produce a first term of 0.056, a change of only 2.3 fold. The second term shows that correction factor is directly proportional to the buffer concentration. The last term, the relationship of the K_a of the buffer to the $[H^+]$, could have the most significant impact on the correction factor.

In the absence of intentionally added H^+ buffers, water and dissolved carbonates can have a significant buffering effect at neutral to alkaline pH (Arif et al. 1995). Water, at a concentration of about 56 M with a Ka of 10^{-16} begins

to impact the correction factor above pH 6. The correction factor due to water acting as a H^+ buffer contributes to the total flux by less than 1% when the pH 6. Bicarbonate in solution, due to atmospheric CO_2, will also have more significant impact at neutral to alkaline pH. Bicarbonate will increase in concentration at more alkaline pH, and can add to the H^+ flux by about 2 and 21% at pH 7 and 8 respectively.

In order to minimize the effect of buffer on H^+ efflux a buffer with a K_a below the $[H^+]$ should be chosen such that most of the buffer will be in its protonated form reducing the effective buffering capacity. As in the former example, investigators can choose buffers to suit their needs, either to remove a very large H^+ flux that is interfering with measurement of other analytes or to correct for the amount of H^+ passing through the plasma membrane in order to accurately quantitate such a flux. See Arif et al. (1995) for a mathematical solution to multiple buffers. This correction method is theoretically applicable to other forms of analyte buffering such as for Ca^{2+} or transition metals.

4.3.6 Other considerations for corrections

In addition to the correction factors discussed above there are other sources of errors that should be addressed. For instance, many plants drive transcellular currents through them, a result of ion transport across single cells or tissues. In low conductivity medium these currents generate substantial voltage gradients next to the cells, coexisting with the chemical gradients of the analytes that we have been discussing. The potentiometric electrodes may sense these small voltage gradients. Therefore the voltage difference measured by the potentiometric electrode will be the sum of the voltage differences due to the analyte concentration difference and the voltage difference based on the current density and medium conductivity. This artifact must be addressed on a sample-to-sample basis. For example, a peak voltage difference during oscillating current influx of about 9 μV would occur over a 10 μm distance immediately in front of a lily pollen tube where current density peaks around 0.4 $\mu A/cm^2$ at a distance of about 20 μm from the cell surface with a medium conductance of about 5000 Ù cm (Messerli and Robinson 1998). This voltage difference is just above the background noise of the system used at that time, ±5 μV for H^+ and Ca^{2+}, ±10 μV for K^+ ISEs (Messerli et al. 1999). The voltage signals due to chemical differences peaked about 6, 10 and 65 times larger for Ca^{2+}, K^+ and H^+ concentration differences, respectively, indicating that the voltage difference could have contributed to the differential analyte concentration by up to 15%, 10% and 1.5% for the Ca^{2+}, K^+ and H^+ measurements, respectively.

In a second example, the electric field determined near the surface of barley roots was considered to be negligible compared to the concentration dependent voltage (Henriksen et al. 1992). While it is important to be aware of such an artifact, in the two cases listed the differential voltage gradient did

little to influence the measured concentration differences. Also medium conductivity can be changed in order to collapse the voltage field without dramatically changing the background concentration of inorganic ions.

The mode of data acquisition itself could lead to underestimates of the true analyte concentration difference. Also, if the response time of the electrodes is slow compared to the acquisition of the differential concentration measurements, the electrode will not be at its steady state value by the time the data has been collected leading to an under measurement of the true concentration difference. As these two corrections are very dependent upon the system electronics and the scheme used for data selection, we will go into more detail about these factors as used on our systems.

4.3.7 Theoretical considerations for signal detection and increased signal to noise

Self-referencing of electrochemical sensors involves the extraction of small electrical signals, μV or fA differences on top of relatively large offset signals, ±100 s mV or ±10–100 s pA. The offset signals are usually large enough that only low-level gain can be used in order to keep the signal within the dynamic range of the amplifier. In order to supply sufficient gain to resolve the small electrical differences either 1) a nearly equal and opposite electrical offset must be supplied before amplification (sample hold mode) or 2) a running average of the low gain measurement can be subtracted from the real-time input before amplification (RC subtract mode). Sample hold mode either applies an offset selected by the user, or collects a voltage at a set point in time from the electrode output. It then applies the same magnitude offset of opposite sign to nullify the offset potential before applying 10^3 times gain. The primary disadvantage for this mode is that drift can take the system back out of the dynamic range of the amplifier so that a new potential must be applied regularly. The advantage is that it does not need an additional correction factor to compensate for the signal lost due to the filtering that occurs in RC subtract mode. In RC subtract mode a high-pass filter is used to collect a running average potential that is subtracted from the potentials collected in the near and far pole. The signals are then amplified 10^3 times before digitizing. We use a high-pass filter that has a time constant of 10 s. Figure 4.4 shows a 200-μV peak to peak square wave input, passed through the BioCurrents Research Center amplifier using Sample Hold and RC subtract mode acquisition. With sample hold mode, the acquired signal is a square wave. The RC subtract mode however, has been distorted due to the filter. RC subtract allows amplification for systems with large drift but involves a correction factor to offset the high-pass filter. The correction factor will be dependent on the time constant of the high-pass filter and the period of data acquisition. For our normal conditions a period of 3.3 s (0.3 Hz translation frequency), 40 μm/s translation speed, 10 s time constant of filter along with data selection of the

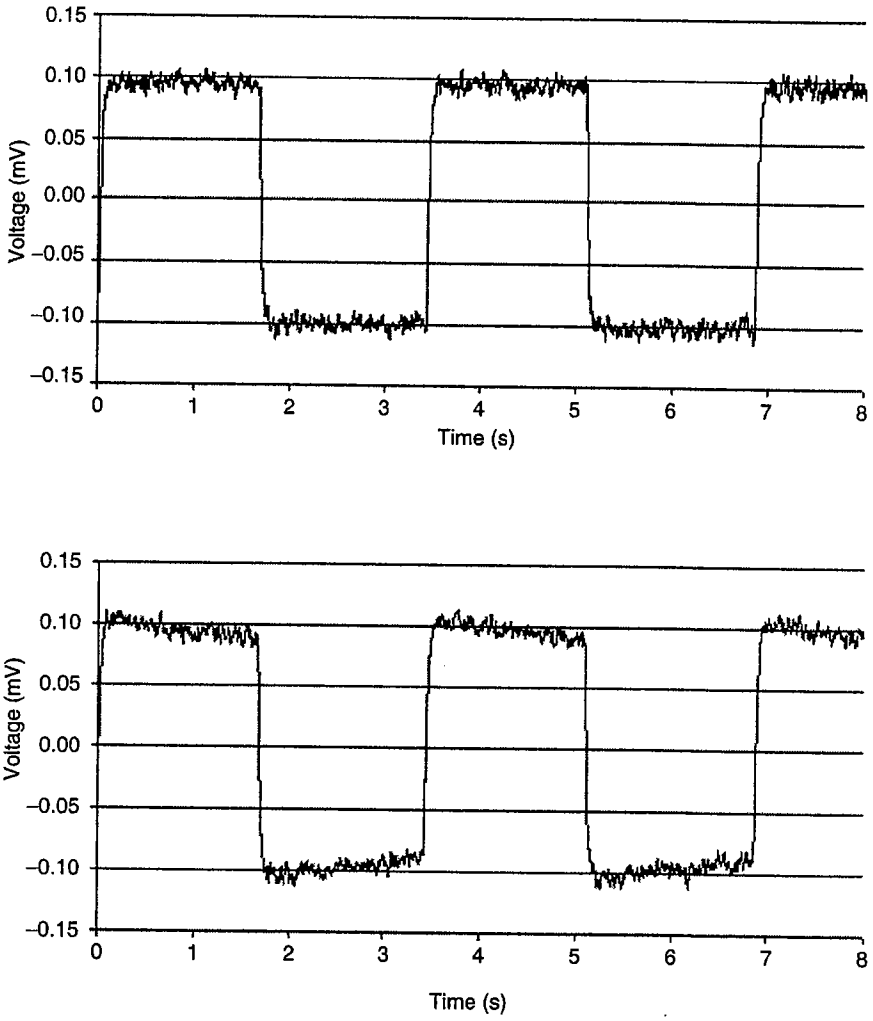

Fig. 4.4. Comparison of the waveform distortion that occurs between "sample hold" and "RC subtract" mode. No distortion occurs for a square wave input during sample hold acquisition mode. The highpass filter used during RC subtract mode does cause waveform distortion that needs to be accounted for when determining the differential concentration

last 70% of the half cycle (more below) we calculate that the signal is 7% smaller than a square wave with similar rise time.

The primary reason for the added level of amplification is to make use of poor resolution digital systems. A dynamic range of ±10 V provides only 4.9 mV/bit resolution for a 12-bit system, and 0.3 mV/bit for a 16-bit system. Therefore, amplification is necessary before digitization to provide adequate bit resolution at or below 1 μV. Now that 24-bit A/D cards exist, signal resolution of 1.2 μV can be attained over a dynamic range of ±10 V.

4.3.8 Data collection

In order to accurately measure the analyte concentration at two points in a gradient with an electrochemical sensor in self-referencing mode, gradient disruption by the electrode must be minimal and the movement time and response time of the electrode must be significantly faster than the excursion period. Gradient disruption will be minimal if a sufficient amount of time is allowed to pass for the gradient to be reestablished after sensor movement, as movement of the sensor may disturb the gradient. The slow movement of the probe, usually, 40 μm/s, does not cause turbulence that can be detected visually. Also, the Reynolds numbers calculated for the speed of movement of either the small tip, 1–4 μm diameter, or even up the shaft where the diameter reaches 50 μm are in the range of 10^{-4} – 10^{-3}, respectively, indicating that only laminar flow occurs around the tip of the sensor. However, if some disturbance does occur, how much time must pass to allow the gradient to be rebuilt? Considering the reestablishment of a K^+ gradient over the excursion distance of the probe, 10 μm, we find that it will only take about 8.3 ms, for K^+ to diffuse this short distance. This indicates that an ionic gradient would be rebuilt in a few tens of milliseconds. As long as turbulent flow does not occur, most small analyte gradients will be rebuilt very quickly.

A second issue to consider is that the sensor must be allowed to remain at each pole of excursion for a period of time long enough for it to acquire a steady state signal. This will inevitably depend on the response times of the sensors. As discussed above, most sensors can reach 95% of their final value within 40–250 ms in physiological solutions. However, contaminants of ISEs can slow the electrode response and cause underestimation of concentration differences. Figure 4.5 shows the voltage response of a H^+-selective electrode, self-referencing near a H^+ sink, in low Ca^{2+} Dickinson's Medium, a culture medium used for growing pollen tubes (Messerli and Robinson 1997). A batch of these electrodes was characterized with the perfusion system and shown to possess an average response time of 223±37 ms with an average Nernstian response of 27.8±0.5 mV between pH 5.5 and 6.0 for a tip size of 1–2 μm listed in Table 4.1. The positional information has been added to the bottom of each graph to show the position and movement of the probe during translation. Figure 4.5 shows that the sensor reaches equilibrium at each

Fig. 4.5. Voltage response of a H^+-selective electrode collected continuously during translation between two position near a H^+ sink. The measurements were acquired in low Ca^{2+} Dickinson's medium. The three graphs correspond to the period of translation listed in the upper right of each trace. The voltage response of the H^+-selective electrode is shown at the top of each graph. The electrode equilibrated quickly with the new position, similar to the response time of the sensor collected in the flow streams listed in Table 4.1. The waveform at the bottom of each graph corresponds to the position of the electrode in the gradient as it changes with time. Translation of the electrode between the two poles is not instantaneous and must be taken into consideration when collecting a differential concentration measurement

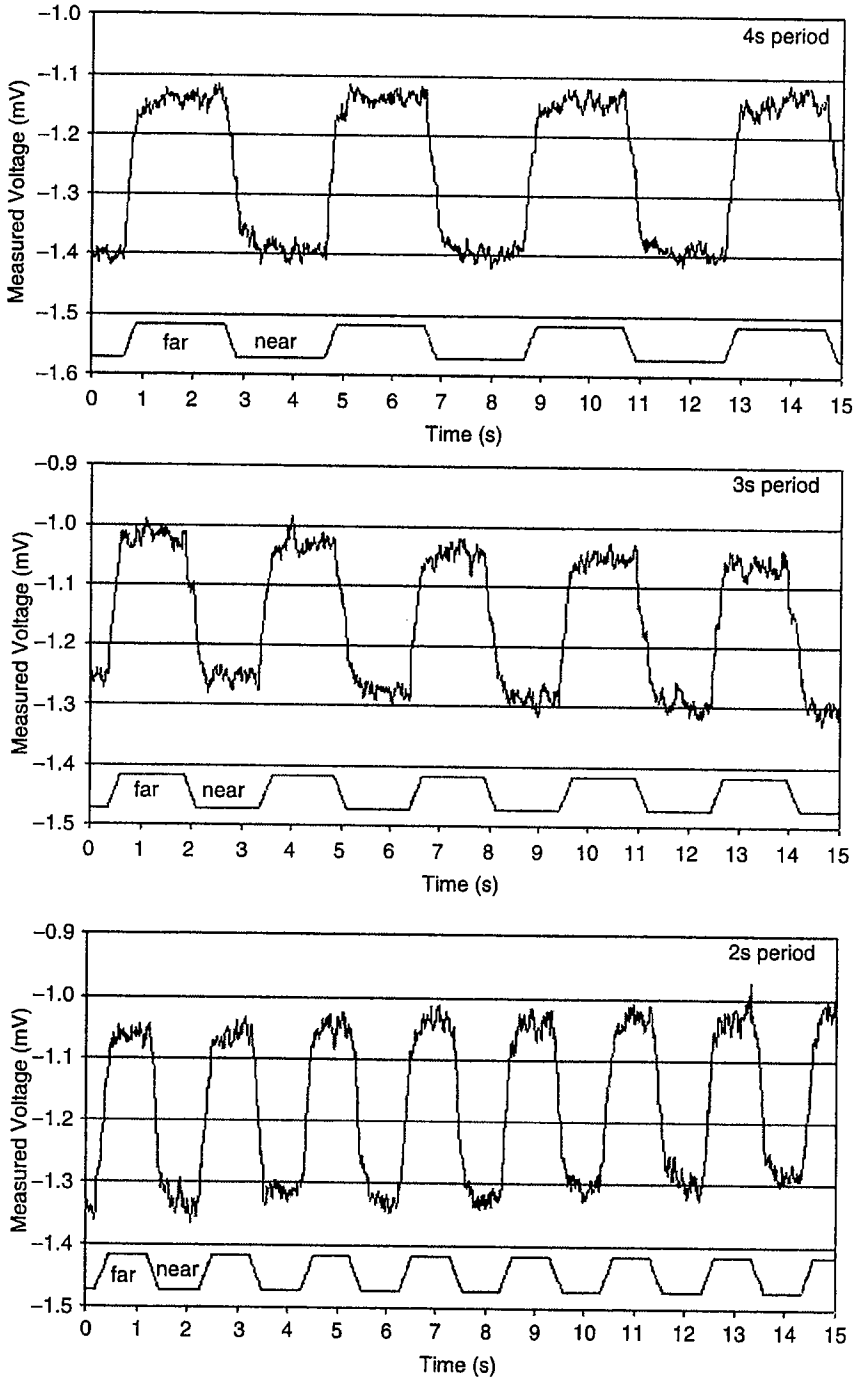

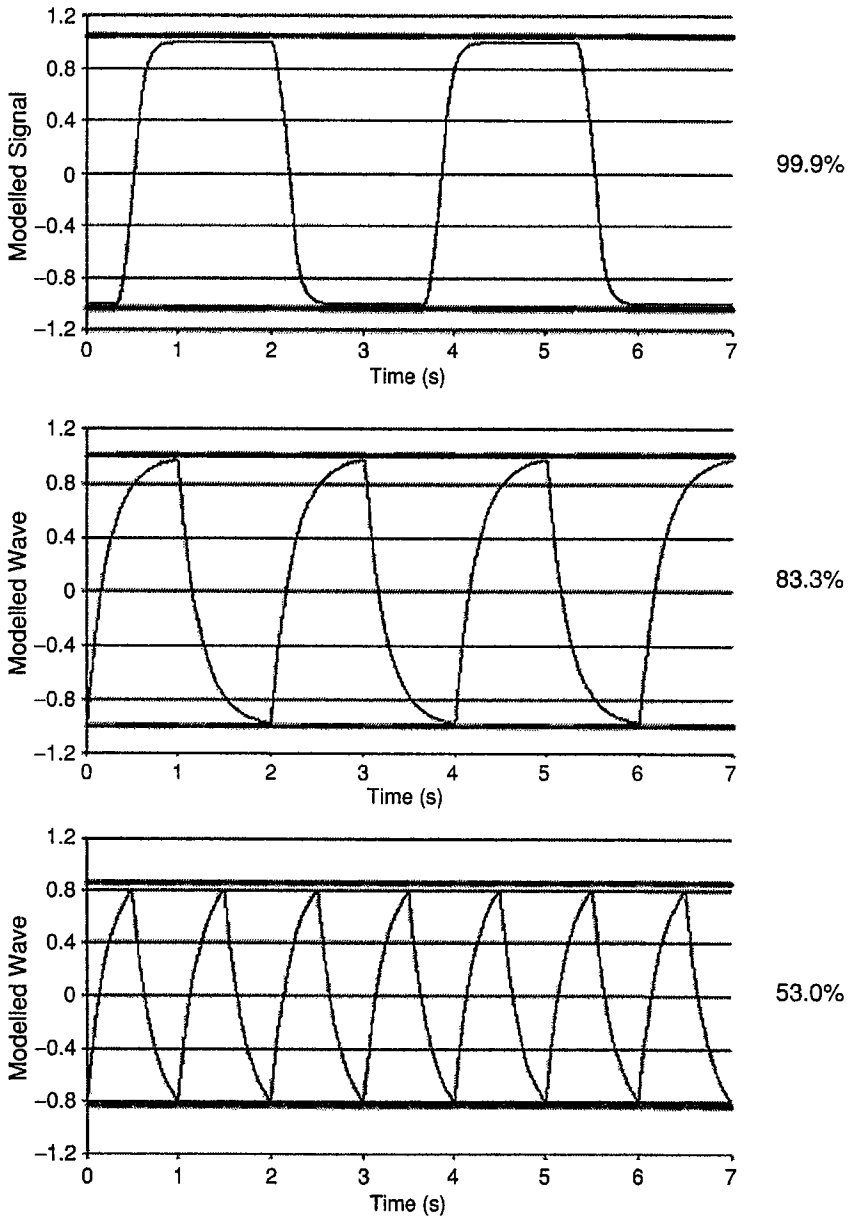

Fig. 4.6. Models of the voltage response for H^+-selective electrodes with different response times and collection periods. The *bars* at the top and bottom of each graph correspond to the 30% of the half cycle that is ignored as it accounts for translation and equilibration (*gray*) while the average of the remaining 70% (*black*) is used to determine a concentration measurement. The *top graph* was generated based on a sensor response time of 223 ms with an excursion time of 250 ms (translation speed 40 μm/s), similar to conditions used by Messerli et al. (1999). The response time is sufficiently fast and these collection parameters allow nearly 100% collection

pole with translation periods of 4, 3 and even 2 seconds because it can reach steady state very quickly. For our typical operating period, 3.3 s, we allow 30% of each half cycle, 0.5 s, for translation and electrode equilibration and then collect the average of the remaining 70%, 1.16 s, to use to determine the concentration. Figure 4.6A shows a model used to calculate the collection efficiency of an acquisition scheme using 250 ms movement time, 223 ms electrode response time and an excursion period of 3.3 s (0.3 Hz) similar to our normal operating parameters. For these parameters the system possesses 99.9% efficiency in collecting the concentration at either pole because the electrode has nearly reached equilibrium before the data has been collected. However, if an electrode was used with a slower response time and/ or a shorter oscillation period, with a similar data collection scheme, a significant underestimation of the concentration difference could result.

A recent example of this may have occurred leading, in part, to a 100–1000 fold discrepancy in H^+ influx at the tips growing pollen tubes (Feijó et al. 1999; Messerli et al. 1999). It must be considered that the cells generate different H^+ fluxes under the different extracellular pH used. However, we also find that there is a technical basis for some of the discrepancy. The parameters for the H^+ selective electrode used by Messerli et al. (1999), are listed above and modeled in Fig. 4.6A. However, with similar diameter electrodes we found that the electrode setup used by Feijó et al. (1999), using their same backfill and pollen tube growth medium along with a 10–15 μm length H^+-selective solvent possess a response time of 572–738 ms for different 0.5 pH steps between pH 5.5–6.5, see Table 4.1. For these studies Feijó et al. (1999) used an oscillation frequency of 0.5–1 Hz and a similar 30:70%, movement and equilibration: data collection scheme. Figure 4.6B and C shows models of the output response based on the average response time over the 5.5–6.5 pH range, 675 ms, during 0.5 Hz and 1 Hz oscillating frequency, respectively. The collection efficiency for the slower response time H^+ electrode at 0.5 Hz is 83.3% of maximum and is only 53.0% of maximum for 1 Hz. For this model, instantaneous translation has been used as no translation speed was listed. Of course the probes are not moved instantaneously and therefore the calculated efficiencies will be significantly lower. The voltage response to a pH change of 5.5–6.5 is only 37.3 ± 0.5 (n=4) indicating that the conditions used by (Feijó et al. 1999) most likely contained an interferent. The slow response times we measured also indicates the presence of an interferent. The conditions used by Feijó et al. (1999) created a subNernstian H^+ electrode with a slower response time giving rise to possible underestimation of the H^+ concentration

---

Fig. 4.6. (*Continued*) efficiency of concentration. The *middle* and *lower graph* correspond to the average response time of the H^+-selective electrode determined in the culture medium used by Feijó et al. (1999) (675 ms) along with the shorter collection periods that they used 2 s (*middle graph*), 1 s (*bottom graph*). The medium causes the electrode to respond more slowly such that it does not reach equilibrium before data collection occurs. This leads to only 83% and 53% efficiency, using the same 30%:70% collection scheme

difference. This case study exemplifies the need to determine the response time and voltage response of the electrode in the medium used and to adjust the collection frequency of the system to accommodate slower sensors. We also encourage investigators to report the voltage/current response and response times of their sensors in order to provide a more solid foundation for independent verification of published results.

4.4 Self-referencing as applied to plants

Among the goals of the plant cell physiologist are the mapping of the movement of ions, metabolites and signaling molecules through the plasma membrane and the determination of the distribution of those ions and molecules within the cell. This section will examine and contrast various physiological techniques with emphasis on self-referencing microelectrodes for accomplishing these goals, as applied to plant cells, and will evaluate those techniques in terms of sensitivity as well as spatial and temporal resolution.

4.4.1 Ca^{2+} fluxes in an alga: comparison of radiotracers and a self-referencing Ca^{2+} electrode

Perhaps the most direct comparison to information obtained with self-referencing measurements is that obtained by the use of tracers, particularly radioactive tracers. Pertinent to the present issue is the use of radioisotopes of small ions to monitor the movement of the ions into or out of cells. Useful tracers exist for Na^+, K^+, Ca^{2+}, Cl^-, SO_4^{2-}, and Mg^{2+}. Often, a radioisotope of Rb^+ has been used as a surrogate for K^+, as it is longer lived and does not emit gamma rays as ^{42}K does. If the flux of an ion into cells is to be measured, the cells are bathed in the tracer at a known specific activity and the amount of the ion that accumulates in the cells in a short time is measured. The length of time of the pulse is constrained on one side by the requirement that the intracellular pool not be significantly labeled so that loss of tracer through backflux will not occur, and on the other side by the need to accumulate a measurable amount of tracer in the cells. It is also possible to load cells with the tracer and then measure the efflux of the labeled ion from the cells. While flux measurements on single cells can be done in the case of certain giant cells, many cells usually must be used to get sufficient accumulation of radioactivity for measurement. Another caveat is the binding of ions to the cell wall; this is especially a problem for divalent cations.

The comparison of fluxes measured with tracers and self-referencing probes can best be illustrated by the case of the Ca^{2+} fluxes in the recently-fertilized eggs of the brown alga, *Silvetia compressa*. Both techniques have been applied to these cells in an effort to understand the role of Ca^{2+} in the establishment of developmental polarity in response to unilateral light. Using ^{45}Ca, it was shown

that the flux of Ca^{2+} into the cells was about 0.15 pmol cm^{-2} s^{-1}, and changed little during the light-induced polarization process (Robinson and Jaffe 1973). By inserting 25,000 cells in a nickel screen, the two hemispheres of the cells could be isolated and flux measurements at the two poles could be measured. It was found that in response to unilateral light, the Ca^{2+} influx became strongly asymmetric, with Ca^{2+} entering the shade, future growth pole, and differentially left the future thallus end (Robinson and Jaffe 1975). These measurements led directly to the prediction that the formation of intracellular Ca^{2+} gradients is an early, essential step in development of polarity.

Recently, the self-referencing Ca^{2+} electrode has been employed to measure net Ca^{2+} fluxes in polarizing *Silvetia* zygotes, affording a direct comparison with the tracer flux data (Pu and Robinson 2003). As noted above, the sensitivity of the self-referencing ion probes declines as the background concentration of the sensed ion increases. In the case of the marine algae, the normal concentration of Ca^{2+} in the sea water is about 10 mM. That proved too high for flux measurements, so it was necessary to culture the cells in 1 mM Ca^{2+}. The cells polarized and germinated normally in the reduced Ca^{2+} medium. The electrode measurements showed that a highly localized region of net Ca^{2+} influx arose during the photopolarization process and was a highly accurate predictor of the locus of the future growth pole. In an individual cell, net influx was measured for a period of one to two hours and had a peak of about 15 pmol cm^{-2} s^{-1}. Net efflux could not be measured anywhere on the cell.

These experiments illustrate both strengths and weaknesses of self-referencing measurements. The locus of net Ca^{2+} influx and its timing could be identified with far more precision using the electrodes, compared to the tracer flux measurements, which required averaging over thousands of cells. However, alterations in the normal medium had to be made in order to carry out the electrode measurements. The electrodes did not detect the predicted asymmetry in efflux, presumably because it is not highly localized like the asymmetric influx. It should be mentioned that a marine cell poses the greatest challenge for self-referencing ion measurements as the background concentration of ions (except protons) is high.

The self-referencing measurement of ion fluxes is vastly more versatile than tracer fluxes. The ability to generate localized flux information using tracers depended on the unique qualities of the fucoid eggs, and the development of specialized techniques with little applicability to other biological systems. The tracer flux measurements also required 15 min to complete while the electrodes have a time resolution of a few seconds.

4.4.2 Evaluation of self-referencing of ion-selective electrodes on pollen tube ion dynamics

Perhaps no other plant system has been the subject of the application of so many different physiological techniques as the pollen tube. The techniques

include radiotracers, autoradiography, self-referencing current and ion flux measurements, voltage and patch clamp measurements and imaging. Thus, the literature on pollen tubes offers a rich array of possibilities for comparing the strengths and limitation of the self-referencing technique to other approaches as well as its ability to complement other approaches. The popularity of the pollen tube as model system stems both from its intrinsic importance in sexual reproduction and the fact that it represents an extreme case of morphological polarity. Pollen tubes can grow as fast as 5 $\mu m\ s^{-1}$ and they achieve this by adding new membrane and cell wall material in a precisely choreographed pattern at the growing tip. There is a strong temporal component, in addition to the spatial one, as growth is oscillatory.

A central role for ions in tip growth was indicated when it was found that Ca^{2+} is an essential component of any medium in which pollen tubes could germinate from the grain and grow (Brewbaker and Kwack 1963). In another early use of the self-referencing voltage probe, it was found that net current of about 0.5 $\mu A\ cm^{-2}$ entered the growing tip of lily pollen tubes (Weisenseel et al. 1975; Weisenseel and Jaffe 1976). Evidence that Ca^{2+} played a controlling role in this current led to the efforts to detect local Ca^{2+} entry using 1 min pulses of ^{45}Ca followed by low temperature (–60 °C) autoradiography of intact pollen tubes (Jaffe et al. 1975). All of the tubes showed accumulation of labeled Ca^{2+} at the tip, and in some cases, intense accumulation was seen.

There has been a resurgence of research on the physiology of pollen tube growth in which self-referencing techniques have played a key role. Ratiometric imaging revealed that there is an obligatory gradient of cytoplasmic Ca^{2+} in growing pollen tubes (Rathore et al. 1991; Miller et al. 1992), with elevated Ca^{2+} at the growing tip. Self-referencing Ca^{2+} electrode measurements showed that there is net Ca^{2+} influx at the growing tip of 1–10 $pmol\ cm^{-2}\ s^{-1}$, and that net influx ceased when growth and Ca^{2+} gradients were disrupted (Kühtreiber and Jaffe 1990; Pierson et al. 1994).

The subsequent finding that growth of pollen tubes is oscillatory (Pierson et al. 1995, 1996) added a temporal dimension to the measurements and it was shown that the Ca^{2+} concentration at the tip also oscillated with the same frequency as growth and nearly the same phase (Holdaway-Clarke et al. 1997; Messerli and Robinson 1997). However, a major discrepancy between the imaging data and the self-referencing Ca^{2+} influx data was evident. The oscillations in electrode-measured influx lagged the oscillations in intracellular Ca^{2+} by about 11 s out of a period of about 40 s (Holdaway-Clarke et al. 1997), a finding that was independently confirmed (Messerli et al. 1999). This discrepancy points out one drawback of the self-referencing electrodes as applied to plants: they cannot distinguish between ions moving into some extracellular sink, such as the cell wall, and true transmembrane flux. Thus, it has not yet been possible to elucidate the connection between the electrode-measured fluxes of Ca^{2+} and the oscillatory changes in cytoplasmic Ca^{2+} in the growing pollen tube.

The fluxes of two other ions have been measured in growing pollen tubes using the self-referencing technique, K^+ and H^+. Messerli et al. (1999) detected large inward oscillations of K^+ at the growing tip. The peaks of these pulses averaged nearly 700 pmol cm^{-2} s^{-1} and lagged the growth peaks by 100°. Clearly, this influx of K^+ is sufficient to have osmotic consequences and may provide a major source of solute for maintaining turgor pressure during rapid volume expansion.

The situation regarding H^+ fluxes is controversial. Messerli et al. (1999) detected large oscillatory proton influx at the tip (peak influx about 500 pmol cm^{-2} s^{-1} for tubes growing at pH 5.5) with smaller influx at least 50 μm behind the growing tip. On the other hand, Feijó et al. (1999) reported much smaller proton fluxes at the tip (about 0.1–1 pmol cm^{-2} s^{-1}) and a very different pattern that included proton efflux in a zone 20–40 μm behind the tip, at least at a medium pH of 6.5. Part of the difference in the magnitudes of the H^+ influx is attributable to the use of a correction factor for the presence of proton buffer in the medium used by Messerli et al. (1999), but that cannot entirely explain the difference. More recently, additional factors have been brought to light that have been discussed above. Specifically, the H^+-selective solvent under the conditions used by Feijó et al. (1999), responded in a subNernstian manner to changes in pH. Additionally the self-referencing frequency was faster and the response time was slower, leading to further possible signal loss. This will have caused Feijó et al. (1999) to greatly underestimate the proton fluxes. It also points to the importance of rigorous electrode calibration in the use of self-referencing electrodes.

Finally, there is a report of large Cl^- efflux from tobacco and lily pollen tubes (Zonia et al. 2002). A critical re-evaluation of that report shows that poor selectivity of the ion-selective solvent (Sigma-Aldrich/Fluka 24899) for the anionic form of the MES buffer that was used, as well as the lack of any Cl^- requirement for growth of lily pollen tubes undermines that claim (Messerli et al. 2004). The sensitivity of the Cl^--selective solvent for the anionic form of MES makes the electrodes indirectly sensitive to the steep pH gradients that exist near the pollen tube tip. These findings underscore the need for careful characterization of electrodes. Much of the published data and manufactures' claims are valid for the media in which animal cells are maintained, but plant cell culture media are quite different and the electrodes require careful evaluation of selectivity in the actual medium used.

The use of the patch clamp technique in various configurations allows the activity and properties of ion channels to be studied. The use of patch clamp requires the removal of the cell wall and necessarily the loss of turgor pressure. Most patch clamp measurements of pollen grains or tubes have utilized the whole-cell configuration with the loss of spatial information (e.g. Griessner and Obermeyer 2003), making direct comparison with extracellular self-referencing measurements difficult. Recently, a successful effort was made to preserve a degree of spatial information in single channel recordings

of patches pulled from defined locations on grain protoplasts or protoplasts from the pollen tube tip (Dutta and Robinson 2004). While three different channels were found on the grain, the only channel that was detected in the tip protoplasts was a stretch-activated (SA) Ca^{2+} channel with properties similar to the SA channel found in the grain. Two types of K^+ channels were found on the grain but no K^+ channels were ever observed on the tip protoplasts. Thus, there is a sharp discrepancy between the patch clamp results and the self-referencing K^+ measurements, which show net K^+ entry of 700 pmol cm^{-2} s^{-1}. Possible explanations are that the measured K^+ influx is not through a channel but a pump, perhaps a K^+/H^+ cotransporter, or the channel localization may be lost due to the disruption of its links to the cytoskeleton in the patch. Whatever the explanation, the self-referencing measurements must be regarded as definitive–, net K^+ influx does occu–, and its mechanism remains to be found. This illustrates the advantages of a non-invasive technique.

4.5 Conclusion

The development of methods for measuring analyte flux with high spatial and temporal resolution extracellular electrochemical sensors has added a vital new dimension to the study of plant physiology. This noninvasive approach has enabled the study of ion transport under normal growing conditions with turgor pressure and cell walls intact. While most of the work has involved monitoring uptake and release of H^+ and inorganic ions with potentiometric sensors, the advances in microscale amperometric detection have enabled the study of a whole new class of analytes, including O_2 and reactive oxygen species. This approach offers considerable promise for the future; for example, the detection of auxin fluxes with subcellular resolution would be a powerful tool in the understanding of how polar auxin transport is organized. As with other physiological tools, continuous characterization of the strengths and weaknesses must occur to prevent misinterpretation of the results. The required characterization can be complex and often take the investigator in unexpected directions. In this review, we have attempted to highlight both the obvious and the more subtle problems with using electrochemical sensors particularly in a time-dependent modulation approach. However, when used properly with good speed and selectivity, the self-referencing approach has opened and will continue to open new avenues in plant research.

References

Ammann D (1986) Ion-selective micro-electrodes, principles, design and application. Springer, Berlin Heidelberg New York

Arif I, Newman IA (1993) Proton efflux from oat coleoptile cells and exchange with wall calcium after IAA or fusicoccin treatment. Planta 189:377–383

Arif I, Newman IA, Keenlyside N (1995) Proton flux measurement from tissues in buffered solution. Plant Cell Environ 18:1319–1324

Baikie ID, Smith PJS, Porterfield DM, Estrup PJ (1999) Multi-tip scanning Bio-Kelvin probe. Rev Sci Instr 70:1842–1850

Bakker E, Bühlmann P, Pretsch E (1997) Carrier-based ion-selective electrodes and bulk optodes. 1. General characteristics. Chem Rev 97:3083–3132

Blüh O, Scott BIH (1950) Vibrating probe electrometer for the measurement of bioelectric potentials. Rev Sci Inst 21:867–868

Bogorff DJ, Messerli MA, Malchow RP, Smith PJ (2003) Development and characterization of a self-referencing glutamate-selective micro biosensor. Biol Bull 205:207–208

Brewbaker JL, Kwack BH (1963) The essential role of calcium ion in pollen germination and pollen tube growth. Am J Bot 50:859–865

Buerk DG (2004) Measuring tissue PO_2 with microelectrodes. Method Enzymol 381:665–690

Crank J (1967) The mathematics of diffusion. Oxford University Press, London

Csöregi E, Quinn CP, Schmidtke DW, Lindquist S-E, Pishko MV, Ye L, Katakis I, Hubbell JA, Heller A (1994) Design, characterization, and one-point in vivo calibration of a subcutaneously implanted glucose electrode. Anal Chem 66:3131–3138

Davies PW (1966) Membrane potential and resistance of perfused skeletal muscle fibers with control of membrane current. Fed Proc 25:332

Demarest JR, Morgan JLM (1995) Effect of pH buffers on proton secretion from gastric oxyntic cells measured with vibrating ion-selective microelectrodes. Biol Bull 189:219–220

Doughty JM, Langton PD (2001) Measurement of chloride flux associated with the myogenic response in rat cerebral arteries. J Physiol 534(3):753–761

Dutta R, Robinson KR (2004) Identification and characterization of stretch-activated ion channels in pollen protoplasts. Plant Physiol 135:1398–1406

Feijó JA, Sainhas J, Hackett GR, Kunkel JG, Hepler PK (1999) Growing pollen tubes possess a constitutive alkaline band in the clear zone and a growth-dependent acidic tip. J Cell Biol 144:483–496

Fleet B, Ryan TH, Brand MJD (1974) Investigations of the factors affecting the response time of a calcium selective liquid membrane electrode. Anal Chem 46:12–15

Friedemann MN, Robinson SW, Gerhardt GA (1996) *O*-Phenylendediamine-modified carbon fiber electrodes for the detection of nitric oxide. Anal Chem 1023:421–425

Garber SS, Messerli MA, Hubert M, Lewis R, Hammar K, Indyk E, Smith PJS (2005) Monitoring Cl^- movement in single cells exposed to hypotonic solution. J Memb Biol 203:101–110

Gow NAR, Kropf DL, Harold FM (1984) Growing hyphae of *Achlya bisexualis* generate a longitudinal pH gradient in the surrounding medium. J Gen Microbiol 130:2967–2974

Grahm L (1964) Measurements of geoelectric and auxin-induced potentials in coleoptiles with a refined vibrating electrode technique. Physiol Plantarum 17:231–261

Grahm L, Hertz CH (1962) Measurement of the geoelectric effect in coleoptiles by a new technique. Physiol Plantarum 15:96–114

Grahm L, Hertz CH (1964) Measurement of the geoelectric effect in coleoptiles. Physiol Plantarum 17:186–201

Griessner M, Obermeyer G (2003) Characterization of whole-cell K^+ currents across the plasma membrane of pollen grain and tube protoplasts of *Lilium longiflorum*. J Membr Biol 193:99–108

Henriksen GH, Raman DR, Walker LP, Spanswick RM (1992) Measurement of net fluxes of ammonium and nitrate at the surface of barley roots using ion-selective microelectrodes. Plant Physiol 99:734–747

Holdaway-Clarke TL, Feijó JA, Hackett GR, Kunkel JG, Hepler PK (1997) Pollen tube growth and the intracellular cytosolic calcium gradient oscillate in phase while extracellular calcium influx is delayed. Plant Cell 9:1999–2010

Jaffe LA, Weisenseel MH, Jaffe LF (1975) Calcium accumulations within the growing tips of pollen tubes. J Cell Biol 67:488–492

Jaffe LF, Levy S (1987) Calcium gradients measured with a vibrating calcium-selective electrode. Proc IEEE/EMBS Conf 9:779–781

Jaffe LF, Nuccitelli R (1974) An ultrasensitive vibrating probe for measuring steady extracellular currents. J Cell Biol 63:614–628

Jung S-K, Hammar K, Smith PJS (2000a) Development of self-referencing oxygen microsensor and its application to single HIT cells. Biol Bull 199:197–198

Jung S-K, Kauri LM, Qian WJ, Kennedy RT (2000b) Correlated oscillations in glucose consumption, oxygen consumption, and intracellular free Ca^{2+} in single islets of Langerhans. J Biol Chem 275:6642–6650

Jung S-K, Trimarchi JR, Sanger RH, Smith PJS (2001) Development and application of a self-referencing glucose microsensor for the measurement of glucose consumption by pancreatic β-cells. Anal Chem 73:3759–3767

Kochian LV, Shaff JE, Kühtreiber WM, Jaffe LF, Lucas WJ (1992) Use of an extracellular, ion-selective, vibrating microelectrode system for the quantification of K^+, H^+, and Ca^{2+} fluxes in maize roots and maize suspension cells. Planta 188:601–610

Kühtreiber WM, Jaffe LF (1990). Detection of extracellular calcium gradients with a calcium-specific vibrating electrode. J Cell Biol 110:1565–1573

Kumar SM, Porterfield DM, Muller KJ, Smith PJ, Sahley CL (2001) Nerve injury induces a rapid efflux of nitric oxide (NO) detected with a novel NO microsensor. J Neurosci 21:215–220

Land SC, Porterfield DM, Sanger RH, Smith PJS (1999) The self-referencing oxygen-selective microelectrode: detection of transmembrane oxygen flux from single cells. J Exp Biol 202:211–218

Lindner E, Gyurcsányi RE, Buck RP (1999) Tailored transport through ion-selective membranes for improved detection limits and selectivity coefficients. Electroanalysis 11:695–702

Mancuso S, Paeschi G, Marras AM (2000) A polarographic, oxygen-selective, vibrating-microelectrode system for the spatial and temporal characterization of transmembrane oxygen fluxes in plants. Planta 211:384–389

Mathison S, Bakker E (1998) Effect of transmembrane electrolyte diffusion on the detection limit of carrier-based potentiometric ion sensors. Anal Chem 70:303–309

Messerli M, Robinson KR (1997) Tip localized Ca^{2+} pulses are coincident with peak pulsatile growth rates in pollen tubes of *Lilium longiflorum*. J Cell Sci 110:1269–1278

Messerli MA, Robinson KR (1998) Cytoplasmic acidification and current influx follow growth pulses of *Lilium longiflorum* pollen tubes. Plant J 16:87–91

Messerli MA, Danuser G, Robinson KR (1999) Pulsatile fluxes of H^+, K^+, and Ca^{2+} lag growth pulses of *Lilium longiflorum* pollen tubes. J Cell Sci 112:1497–1509

Messerli MA, Smith PJS, Lewis RC, Robinson KR (2004) Chloride fluxes in lily pollen tubes: a critical reevaluation. Plant J 40:799–812

Miller DD, Callaham DA, Gross DJ, Hepler PK (1992) Free Ca^{2+} gradient in growing pollen tubes of Lilium. J Cell Sci 101:7–12

Nuccitelli R (1991) Vibrating probe technique for studies of ion transport. In: Foskett JK, Grinstein S (eds) Noninvasive techniques in cell biology. Wiley-Liss, New York, pp 273–310

Pepperell JR, Porterfield DM, Keefe DL, Behrman HR, Smith PJS (2003) Control of ascorbic acid efflux in rat luteal cells: role of intracellular calcium and oxygen radicals. Am J Physiol 285:C642–C651

Pergel E, Gyurcsanyi RE, Toth K, Lindner E (2001) Picomolar detection limits with current-polarized Pb^{2+} ion-selective membranes. Anal Chem 73: 4249–4253

Phillips PEM, Wightman RM (2003) Critical guidelines for validation of the selectivity of in-vivo chemical microsensors. Trends Anal Chem 22:509–514

Pierson ES, Miller DD, Callaham DA, Shipley NM, Rivers BA, Hepler PK (1994) Pollen tube growth is coupled to the extracellular calcium ion flux and the intracellular calcium gradient: effect of BAPTA-type buffers and hypertonic medium. Plant Cell 6:1815–1828

Pierson ES, Li YQ, Zhang GQ, Willemse MTM, Liskens HF, Cresti M (1995) Pulsatory growth of pollen tubes: investigation of a possible relationship with the periodic distribution of cell wall components. Acta Bot Neerl 44:121–128

Pierson ES, Miller DD, Callaham DA, van Aken J, Hackett G, Hepler PK (1996) Tip-localized calcium entry fluctuates during pollen tube growth. Dev Biol 174:160–173

Pineros MA, Shaff JE, Kochian LV (1998) Development, characterization and application of a cadmium-selective microelectrode for the measurement of cadmium fluxes in roots of *Thlaspi* species and wheat. Plant Physiol 116:1393–1401

Porterfield DM, Laskin JD, Jung S-K, Malchow RP, Billack B, Smith PJS, Heck DE (2001) Proteins and lipids define the diffusional field of nitric oxide. Measurement of nitric oxide fluxes from macrophages using a self-referencing electrode. Am J Physiol 281:L904–L912

Pu RS, Robinson KR (2003) The involvement of Ca^{2+} gradients, Ca^{2+} fluxes, and CaM kinase II in polarization and germination of *Silvetia compressa* zygotes. Planta 217:407–416

Rathore KS, Cork RJ, Robinson KR (1991) A cytoplasmic gradient of Ca^{2+} is correlated with the growth of lily pollen tubes. Dev Biol 148:612–619

Robinson KR, Jaffe LF (1973) Ion movements in a developing fucoid egg. Dev Biol 35:349–361

Robinson KR, Jaffe LF (1975) Polarizing fucoid eggs drive a calcium current through themselves. Science 187:70–72

Sanger R, Karplus E, Jaffe LF (1990) An aerial vibrating probe. Biol Bull 179:225

Schneiderman G, Goldstick TK (1976) Oxygen fields induced by recessed and needle oxygen microelectrodes in homogenous media. Adv Exp Med Biol 75:9–16

Schneiderman G, Goldstick TK (1978) Oxygen electrode design criteria and performance characteristics: recessed cathode. J Appl Physiol 45:145–154

Shabala S, Newman I (1998) Light-induced changes in hydrogen, calcium, potassium, and chloride ion fluxes and concentrations from the mesophyll and epidermal tissues of bean leaves. Understanding the ionic basis of light-induced bioelectrogenesis. Plant Physiol 119:1115–1124

Shabala S, Babourina O, Newman I (2000) Ion-specific mechanisms of osmoregulation in bean mesophyll cells. J Exp Bot 51:1243–1253

Smith PJS, Hammar K, Porterfield DM, Sanger RH, Trimarchi JR (1999) Self-referencing, non-invasive, ion selective electrode for single cell detection of trans-plasma membrane calcium flux. Microsc Res Techniq 46:398–417

Twig G, Jung S-K, Messerli M, Smith PJS, Shirihai O (2001) Real-time detection of reactive oxygen intermediates from single microglial cells. Biol Bull 201:261–262

Twig G, Graf SA, Messerli MA, Smith PJS, Yoo SH, Shirihai OS (2005) Synergistic amplification of beta-amyloid- and interferon-gamma-induced microglial neurotoxic response by the senile plaque component chromogranin A. Am J Physiol 288:C169–C175

Weisenseel MH, Jaffe LF (1976) The major growth current through lily pollen tubes enters as K^+ and leaves as H^+. Planta 133:1–7

Weisenseel MH, Nuccitelli R, Jaffe LF (1975) Large electrical currents traverse growing pollen tubes. J Cell Biol 66:556–567

Whalen WJ, Riley J, Nair P (1967) A microelectrode for measuring intracellular PO_2. J Appl Physiol 23:798–801

Zhang X, Kislyak Y, Lin J, Dickson A, Coradosa L, Broderick M, Fein H (2002) Nanometer size electrode for nitric oxide and S-nitrosothiols measurement. Electrochem Commun 4:11–16

Zonia L, Cordeiro S, Tupy J, Feijó JA (2002) Oscillatory chloride efflux at the pollen tube apex has a role in growth and cell volume regulation and is targeted by inositol 3,4,5,6-tetrakisphosphate. Plant Cell 14:2233–2249